Article

Phosphorene Nanosheets Exfoliated from Low-Cost and High-Quality Black Phosphorus for Hydrogen Evolution

Weihan Li,[#] Minsi Li,[#] Junjie Li, Jianneng Liang, Keegan R. Adair, Yongfeng Hu, Qunfeng Xiao, Xiaoyu Cui, Ruying Li, Frank Brandys, Ranjith Divigalpitiya, Tsun-Kong Sham,* and Xueliang Sun*
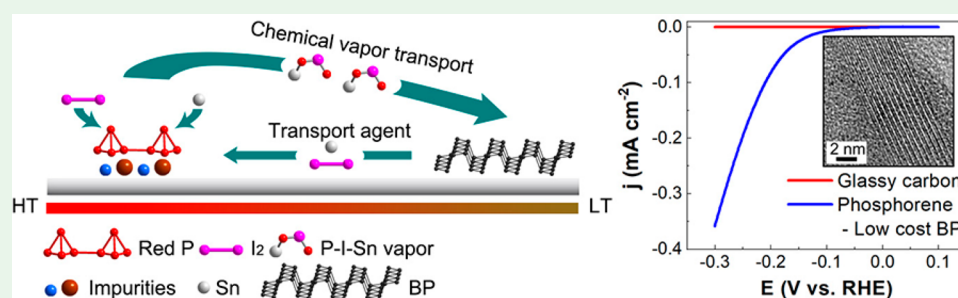
Read Online

ACCESS | 📊 Metrics & More | 📰 Article Recommendations | 🆘 Supporting Information

ABSTRACT: Black phosphorus (BP) has recently attracted intense research interest due to its unique thickness-dependent and anisotropic electronic and photonic properties, and has shown promising potential in nanophotonic, nanoelectronics and energy storage applications. However, the application of BP in practical devices is hindered by its high commercial cost. To further reduce the cost and accelerate the development of BP, a highly efficient preparation strategy for low-cost BP must be found. Herein, we report such a method via a modified chemical vapor transport (CVT) method by replacing high-purity red phosphorus (RP) with a low-purity precursor counterpart. We show that this method can drastically reduce the cost of manufacturing by several orders of magnitude. Furthermore, the BP produced using low-cost RP shows nearly the same crystal quality, high purity, local chemical structure, and electronic properties, compared with those of the high-cost BP prepared by the traditional CVT method. Most importantly, exfoliated phosphorene nanosheets prepared from the low-cost BP exhibit promising hydrogen evolution reaction (HER) activity. Owing to the high quality and high conversion efficiency, the low-cost BP holds promising potential in future scientific research and industrial applications.

KEYWORDS: low-cost black phosphorus, red phosphorus, CVT, exfoliation, HER

1. INTRODUCTION

Black phosphorus (BP) was first prepared in 1914 by Percy W. Bridgman and has recently been rediscovered as a novel two-dimensional (2D) layered material that can be exfoliated into single-layer/few-layer sheets, denoted as "phosphorene".[1−3] The revival of BP lies in its unique properties, especially the thickness-dependent and anisotropic characteristics. Different from other 2D materials (e.g., graphene, transition metal dichalcogenides (TMDs), and hexagonal boron nitride (hBN)), BP exhibits a thickness-dependent electronic band structure with a tunable direct bandgap (from ∼0.3 eV in a bulk structure to ∼2.0 eV in a monolayer structure) and a charge-carrier mobility (up to 1000 cm² V⁻¹ s⁻¹ for a thickness of ∼10 nm).[4,5] Furthermore, BP displays exciting advantages over graphene, TMDs, and hBN owing to its strong in-plane anisotropic electrical, thermal, optical, and phonon properties, resulting from the lower symmetry of the puckered layer structure.[6−9] These unique physical properties provide promising opportunities for its wide applications in nano-photonics, nanoelectronics, optoelectronics, and energy

devices, such as a hydrogen evolution reaction (HER) and an oxygen evolution reaction (OER).[6,10−16] However, the application of BP in practical devices is hindered by two factors: the fast degradation of phosphorene upon exposure to air and the extremely high cost of commercially available BP single crystals.[17,18]

In the case of the degradation behavior of BP, several groups have studied the degradation mechanism and provided several protection strategies (e.g., passivation layers and doping with heteroatoms) for bulk BP and phosphorene.[19−23] To address the high cost, significant efforts have been put forward to find suitable methods to synthesize large-scale and low-cost BP.
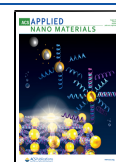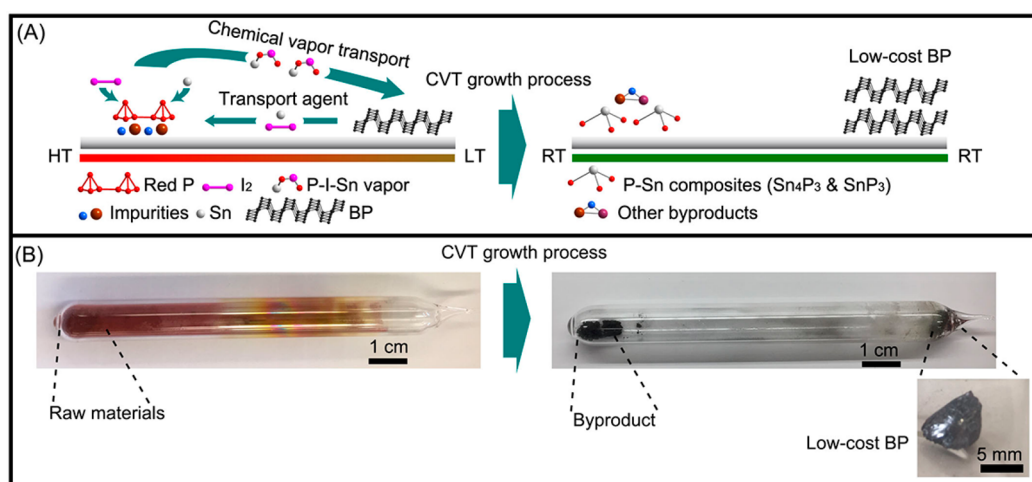
Figure 1. (A) Schematic illustration of the modified CVT process used to grow low-cost BP. (B) Digital photographs of the sealed silica ampule with low-purity RP as the precursor before and after the CVT growth process. The inset in part B shows a magnified photograph of the obtained low-cost BP.

Following the high-pressure method by Percy W. Bridgman in 1914, large BP single crystals (several millimeters cubed) were prepared using a wedge-type cubic anvil or multianvil-type high-pressure apparatus.[24,25] The large BP crystals obtained from this method are ideal for the study of specific physical and chemical properties. However, the high-pressure method relies on a specialized and complicated apparatus, and it is not suitable for wide utilization and large-scale industrial applications. In addition to the high-pressure method, mercury catalysis and bismuth flux methods have also been deemed to be unviable due to either being ecologically damaging, too complicated, and/or time-consuming.[26,27] To achieve an easy, eco-friendly, and efficient way to synthesize BP, Nilges et al. in 2008 developed a facile and fast chemical vapor transport (CVT) strategy to prepare large BP crystals using red phosphorus (RP), Sn–Au alloy, and SnI_4 as mineralization additives, which shortened the growth process from 5–10 days to 70 h.[28,29] The Nilges group later improved the preparation process using Sn and SnI_4, resulting in a drastic reduction of side phases.[30] In addition to the successful preparation of BP crystals by the CVT method, H. Zhang, A. Pan, and K. Zhang et al. realize the preparation of BP films on silicon substrates via a gas phase growth strategy.[31] Via an epitaxial nucleation design, the thickness of BP films is controllable after a further lateral growth control. While the CVT strategy enables the preparation of BP with an affordable price (around $600 (USD)/g) for specific research, the cost of BP crystals is still a crucial barrier for industrial and large-scale applications.[18]

To further reduce the cost of BP crystals, the rational design of a modified CVT method based on Nilges' work should be considered for BP growth.[28−30] In 2016, two groups reported a similar strategy to reduce the cost of BP preparation by replacing the SnI_4 mineralizer in the earlier procedure with iodine (I_2).[32,33] Experimental information and the calculation to follow confirm the key role of I_2 and Sn in the successful synthesis of BP.[34,35] Until now, all previous modification strategies of the CVT method aiming to reduce the cost of BP have focused on the mineralizers in BP crystal growth. Nevertheless, only a small amount of the mineralizer (e.g., I_2 or SnI_4) was applied in BP crystal growth (tenths to hundredths of a milligram), and it is not the dominant factor in the cost of BP. RP is the main factor controlling the final cost of BP (white phosphorus is ruled out due to its highly reactive, pyrophoric, and extremely dangerous characteristics). To the best of our knowledge, all previous reports showing successful preparation of high-purity BP via the high-pressure or CVT methods always utilized high-purity RP (99.99− 99.999+%, trace metal basis) as the precursor. High-purity RP is high in cost and unacceptable for large-scale industrial application. Additionally, previous work also confirms that there are still several impurities in BP prepared through the CVT method, which need modification to reduce the percentage of the impurity inside.[36] Therefore, it would be more beneficial to use low-cost RP, such as commercially available low-purity RP (e.g., 97−99%, trace metal basis), to prepare high-quality BP with a low cost. The main obstacle for the utilization of low-purity RP is the impurities (e.g., Fe, Mg, and O), which should be absent from the grown BP products. Considering the two main BP preparation methods, it is immediately apparent that, while the impurities cannot be removed from the final BP products prepared via the high-pressure method, it is entirely possible to realize the exclusion of impurities via the CVT method if the impurities would not participate in the vapor transport process.

Herein, we report a modified CVT method using low-purity RP as the precursors and Sn and I_2 as mineralization additives, by which we have realized a highly efficient preparation method for low-cost BP. Using a modified CVT method, we have prepared large and high-quality BP crystals from the low-purity RP in a moderate period of time. Additionally, no noticeable impurities in the low-purity RP have been transported to the final BP products, while nearly 97% of RP has been converted to BP, ensuring the high purity level of the BP crystals with a high conversion efficiency. Most importantly, the utilization of low-purity RP can drastically reduce the cost by several orders of magnitude over that of the BP prepared from high-purity RP. Based on the low-cost BP, exfoliated phosphorene nanosheets have also been prepared, showing promising HER activity. Thus, this modified CVT method shows promising potential in future scientific research and industrial applications.
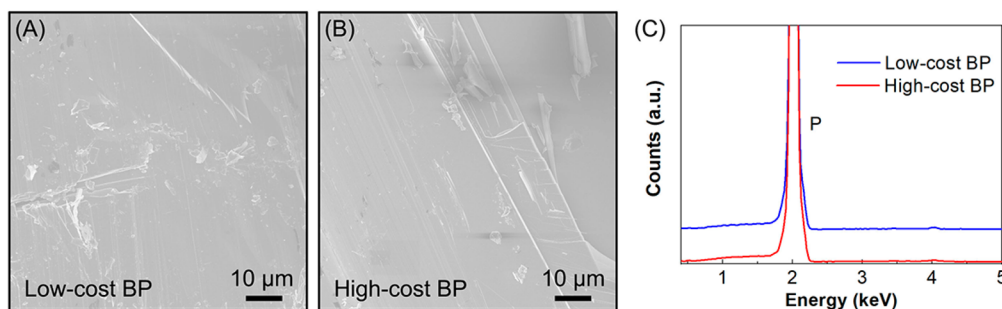
Figure 2. SEM images of (A) low-cost BP and (B) high-cost BP crystals and (C) EDX result of both BP crystals.

2. RESULT AND DISCUSSION

Herein, we describe a modified CVT method that can produce high-quality BP with a high conversion efficiency. In this study, we tracked the growth mechanism of this method by comparing the characteristics of BP crystals prepared from low-purity RP to those of crystals prepared from high-purity RP. The low-purity (≥97%, trace metal basis) and high-purity RPs (≥99.99%, trace metal basis) were used for BP crystal growth as purchased, without further purification. Both display the typical crystal structure of amorphous RP (see the Supporting Information, Figure S1). Figure S1A shows the X-ray diffraction (XRD) patterns of low-purity and high-purity RPs; both exhibit similar patterns with four broad peaks at 2θ ≈ 15, 32, 42, and 55°. The very broad peaks suggest the presence of a medium-range structural order in both RPs, in accordance with the Raman spectra shown in Figure S1B.[37] Both RPs display the typical wide Raman peaks between 200 and 500 cm^{-1} of red phosphorus with a similar intensity, suggesting similar disordered crystal structures.[38]

In the case of the impurities in low-purity RP, scanning electron microscopy (SEM) combined with energy-dispersive X-ray spectroscopy (EDX) was carried out to study the morphology and composition of both high- and low-purity RP. As shown in Figure S2A,B, both low-purity and high-purity RPs present polygon-type morphologies with the size ranging from 1 to 20 μm. Additionally, based on the EDX result shown in Figure S2C, high-purity RP displays only phosphorus with just one sharp peak at around 2 keV (P Kα), indicating no obvious impurities. However, the low-purity RP, as expected, shows several obvious impurities, including O, Fe, Na, Mg, Al, and Ca, resulting from the preparation and storage process of commercial RP.[39] Furthermore, the impurities are uniformly distributed based on the EDX spectra (see the Supporting Information, Figure S3).

Figure 1A displays the schematic of the modified CVT process with low-purity RP as the precursor and Sn and I$_2$ as the mineralizer additives. All raw materials were sealed in quartz ampules under a vacuum, which were then placed in the furnace with a temperature gradient. As discussed above, I$_2$ and Sn have been confirmed to be a pair of effective mineralizer additives which can transport phosphorus from the high-temperature (HT) side to the low-temperature (LT) side and facilitate the BP crystal growth (Figure 1).[35] Because the impurities cannot participate in the CVT process, the impurities (including Sn$_4$P$_3$, SnP$_3$, and other impurities) located at the HT side were naturally separated from the BP crystal grown at the LT side when the temperature lowers down to room temperature (RT). Figure 1B shows the digital photograph of the sealed quartz ampules with the raw

materials, displaying a mixture of yellow and red color on the inner surface of ampules owing to the sublimation at a high temperature and the deposition of P and I$_2$. Figure 1B also shows the digital photograph of the quartz ampule after BP growth, where it can be seen that BP crystals with a cone shape (around 5 mm in size) were grown at the LT side, while the black-colored byproduct formed from the impurities in RP was left at the HT side. Because the grown BP crystals and the byproduct are gathered in the opposite sides in the quartz tube, they can be easily separated by breaking the quartz tube into two parts. Then the grown BP crystals were peeled off the quartz tube. Therefore, BP crystals can be synthesized from low-purity RP via the modified CVT process, and impurities can be separated from the product. Thus, the use of low-purity RP can drastically reduce the overall cost to an affordable level. BP crystals prepared from low-purity RP are henceforth denoted as low-cost BP. The high-purity RP was used to grow BP crystals via the CVT method under the same growth parameters, denoted as high-cost BP, for comparison.

As shown in Figure S4, high-cost BP was also synthesized at the LT side with the gray metal-colored byproduct left at the HT side, which is different from the black-colored byproduct formed during the low-cost BP growth process (Figure 1B). As shown in Figure S5A,B, the byproduct of the low-cost BP shows a spherical morphology (diameter ~40 μm) mixed with other smaller particles with the compositions of O, Fe, Na, Mg, Al, and Ca originating from the impurities in low-cost RP, I, and Sn from the CVT process. The EDX of the byproduct indicates that the impurities did not participate in the CVT process and were left at the raw material side after BP growth. The reason why the impurities in the high-purity RP raw materials cannot participate in the CVT growth process is related to the reaction mechanism. The elements (e.g., P) that can participate in the CVT growth should form iodides during the heating process. The elements of the impurities in the high-purity RP raw materials cannot form corresponding iodides, resulting in the impurities that cannot participate in the BP growth process and the absence of impurity elements in the final low-cost BP products. The impurities were left at the starting material side. Elemental iodine has not been detected, possibly because of its volatile nature. Compared with the byproduct of the high-cost BP, that of the low-cost BP shows similar crystalline Sn–phosphide phases of Sn$_4$P$_3$ and SnP$_3$, which is in accordance with previous reports (Figure S5C).[30,34] In the case of the byproduct of low-cost BP, no crystalline impurity phases have been detected.

Upon separating BP crystals from the byproducts, one low-cost BP crystal with the mass of 0.1874 g was obtained with a high conversion efficiency of ~96.6 wt % based on the phosphorus composition in low-purity RP, which is almost the
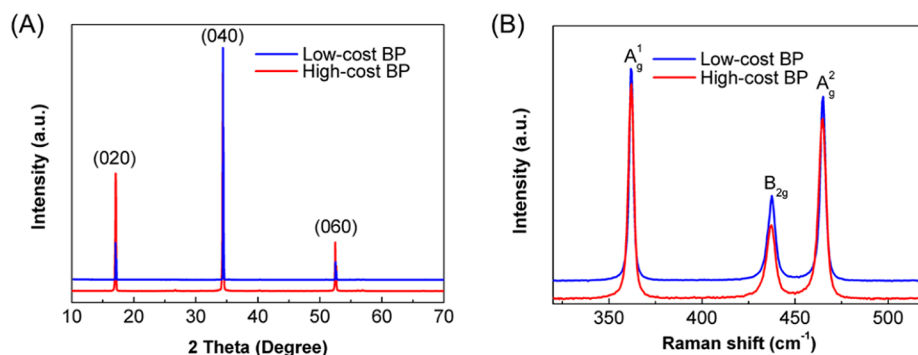
Figure 3. (A) XRD patterns and (B) Raman spectra of low-cost BP and high-cost BP crystals.
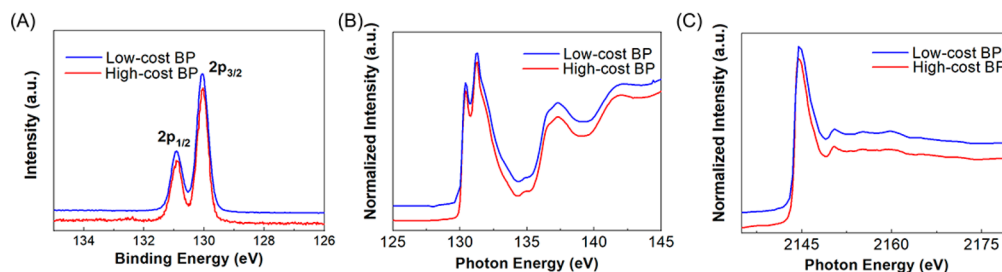

Figure 4. (A) Synchrotron-based P 2p XPS spectra (excitation photon energy = 240 eV), normalized XANES spectra acquired with the TEY mode at the (B) P $L_{2,3}$-edge and the (C) P K-edge of low-cost BP and high-cost BP.

same as that of high-cost BP (Figure S6). The reason why the conversion ratio is calculated based on the P weight in the starting materials is that this calculation can provide more accurate chemical reaction information. Regarding the cost of low-cost and high-cost BP preparation, the cost of low-cost BP is around 255 times lower than that of high-cost BP based on the price of RP precursors (high-purity RP = $28 (USD)/g, low-purity RP = $0.11 (USD)/g). The high conversion efficiency indicates that the impurities in low-purity RP do not affect the CVT process, making it entirely feasible to use low-purity RP to grow BP crystals via the CVT method. Furthermore, the produced low-cost BP shows the same crystal quality compared with that of high-cost BP. As shown in Figure 2A,B, both BP crystals display a clean surface without obvious mineralizer residuals. Additionally, the EDX spectra shown in Figure 2C confirms the purity in both the low-cost and high-cost BP, showing no noticeable impurities from the low-purity RP starting material (Figure S2). In particular, no oxygen has been found in the low-cost BP, while elemental oxygen is one of the main compositions in the low-purity RP starting materials. The reason is also related the modified CVT growth process. Because elemental oxygen in the low-purity RP should come from impurities, such as metal oxides, it cannot participate the BP growth process. The absence of oxygen in the obtained low-cost BP crystals makes the materials one promising candidate material for practical application in nanophotonics and nanoelectronics. Furthermore, the impurity level of low-cost BP has been quantified via inductively coupled plasma mass spectrometry (ICP-MS), exhibiting a high purity level of ∼99.9 at. %, which is similar to that of the high-cost BP. To further confirm the purity level of the obtained low-cost BP, we carried out X-ray photoelectron spectroscopy to get the detailed chemical information regarding different elements, including P, Sn, and I. As shown in Figure S7 (see the Supporting Information), clear peaks belonging to P 2s and 2p peaks can be found while the

intensity of the peaks belonging to Sn and I is negligible, indicating the very low impurity level in the final BP product. The phosphorus content in the low-cost BP is around 99 wt % and is calculated based on the XPS peak intensity. The purity level of our low-cost BP is consistent with that of the previous BP crystal growth results.[29,30] The purity level determines the electrical properties of BP crystals, which has a crucial influence on the application in electronics. We used a four-point probe to test the electrical conductivity of low-cost and high-cost BP crystals, as shown in Figure S8 (see the Supporting Information). The electrical conductivities of the low-cost and high-cost BP crystals are 72 and 74 S/m, respectively, which is consistent with the previous reports.[40,41] The similar electrical conductivities of the low-cost and high-cost BP crystals indicate the similar high purity levels. Because this modified CVT method can use low-purity RP as raw materials to prepare BP crystals, it is reasonable to control the defect and doping concentrations in the final products. As there are already several works that reported the preparation of Se, or S-doped BP,[42,43] it is reasonable to introduce dopant elements in the raw materials, such as Se or S powder, which can participate in the BP crystal growth process. The concentration of defects and the doping concentration can be controlled by modifying the amount of Se or S powder in raw materials, and it can also be controlled by modifying the growth temperature and time.

Figure 3A shows the X-ray diffraction (XRD) patterns of the low-cost BP and high-cost BP, exhibiting the same three main peaks located in the same positions, corresponding to (0k0) of BP's orthorhombic crystalline orientation.[30,34] Moreover, the sharp XRD peaks in both patterns indicate a high crystal quality without crystalline impurities in both BP crystals, which is consistent with the Raman spectra shown in Figure 3B. Both BP crystals display three main peaks, corresponding to the typical high-frequency Raman modes (A_g^1, B_{2g}, and A_g^2) and the same high degree of crystallinity.
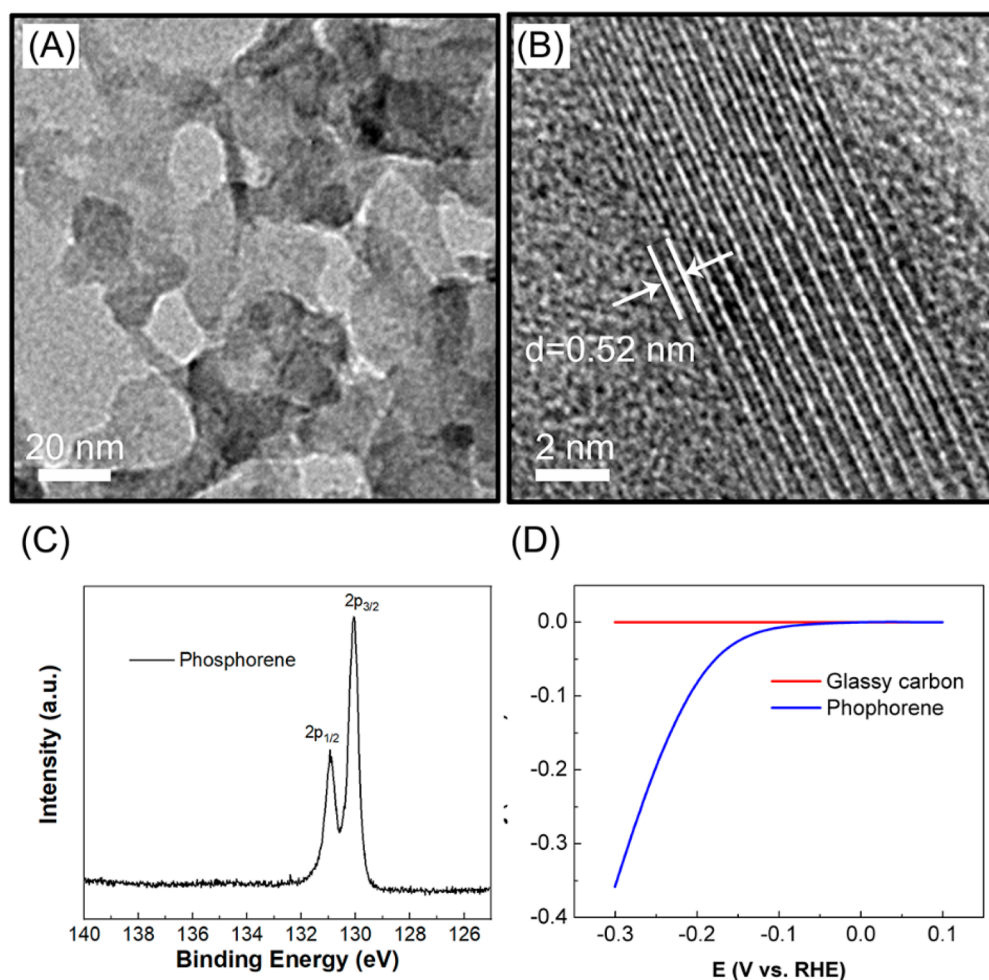
Figure 5. (A) TEM image, (B) HRTEM image, (C) synchrotron-based P 2p XPS spectra (excitation photon energy = 240 eV) of phosphorene nanosheets, and (D) LSV curves of phosphorene catalyst for hydrogen evolution in 0.1 M HClO$_4$.

In addition to the crystal structure, the local chemical environment of low-cost BP has also been studied by synchrotron-based P 2p X-ray photoelectron spectroscopy (XPS).[44,45] P 2p XPS measurements were carried out using the excitation photon energy of 240 eV, which is highly surface-sensitive (probing depth of around 0.5 nm, because the kinetic energy of P 2p peaks of ~105 eV is near the minimum of the universal electron escape depth). As shown in Figure 4A, two XPS peaks at around 130.06 and 130.94 eV represent the P 2p$_{3/2}$ and 2p$_{1/2}$ core levels with a spin−orbit split of ~0.88 eV. Based on previous XPS studies of degraded BP, oxidized BP always shows additional 2p XPS peaks at a higher binding energy, corresponding to phosphorus oxides or phosphate (e.g., 135 eV).[46] However, low-cost BP only shows two XPS peaks without the additional phosphorus oxide peaks, indicating its high chemical purity without degradation on the surface. Furthermore, the local chemical and electronic structures have been studied by X-ray absorption near the edge structure (XANES) at the P L$_{2,3}$- and K-edges (Figure 4B,C) acquired by the total electron yield (TEY) mode, showing probing depths of ~5 nm and of about tens of nanometers, respectively, tracking the densities of states above the Fermi level with 3d and 3s and 3p transitions, respectively. Consistent with the P 2p XPS, the first two peaks at the P L$_{2,3}$-edge XANES spectrum of low-cost BP correspond to electron transitions from 2p$_{3/2}$ and 2p$_{1/2}$ orbitals to the unoccupied 3d

orbital and 4s states above the Fermi level, according to the dipole selection rules, while other peaks at a higher photon energy might be due to multiple scattering effects.[47,48] In the case of the P K-edge XANES spectrum of low-cost BP, one absorption peak with the white line at around 2145.2 eV is related to the electron transition from the P 1s orbital to the unoccupied 3p state.[47] Compared to those of XPS, XANES spectra are sensitive to both the oxidation state and coordination environment of P. Furthermore, the XANES spectra of low-cost BP at both P L$_{2,3}$- and K-edges show typical features of standard BP, indicating a high crystal quality without obvious oxide defects. Compared with the high-cost BP, low-cost BP shows the same XPS and XANES spectra, suggesting the same crystal quality with the same local and electronic structure in both BP crystals, and the as-prepared crystal appears to be less susceptible to degradation. Compared with previously prepared BP crystals,[29,32,33] the prepared BP crystal in our work shows a high elemental purity, good crystalline degree, and reasonable electronic structure which is confirmed by several characterization methods, including SEM-EDX, ICP, XRD, Raman, XPS, and XANES. Therefore, it is reasonable to confirm the high quality of the prepared BP crystals.

Owing to the extremely low cost of this modified CVT method, low-cost BP shows great promise for future applications. Various applications of BP including nano-

photonics, nanoelectronics, energy storage devices, and catalysis are mainly based on exfoliated phosphorene, such as the hydrogen evolution reaction (HER) and oxygen evolution reaction (OER).[10−12] To explore the HER activity of the low-cost BP, phosphorene was prepared through liquid exfoliation in N-Methyl-2-pyrrolidone (NMP). The thickness can also be controlled by tuning the centrifugation speed (see the Experimental Section in the Supporting Information). Figure 5A shows the transmission electron microscopy (TEM) image of the prepared phosphorene, displaying a nanosheet morphology with sizes from 20 to 50 nm. The clean and smooth surface of the obtained phosphorene indicates no obvious impurities and oxidation after the exfoliation process.[17] Additionally, high-resolution TEM (HRTEM) images of the edge section exhibits a typical crystalline structure with a lattice spacing of 0.52 nm corresponding to the (020) crystal plane (Figure 5B). The total thickness of the selected edge of phosphorene is around 10 layers. To further confirm the chemical information, the obtained phosphorene was also studied by the synchrotron-based P 2p X-ray photoelectron spectroscopy (XPS). As shown in Figure 5C, two XPS peaks at around 130.06 and 130.94 eV represent the P $2p_{3/2}$ and $2p_{1/2}$ core levels with a spin−orbit split of ∼0.88 eV without any peaks at a higher photon energy, indicating the absence of the oxidation of phosphorene during the exfoliation process.[49] Furthermore, the HER catalytic activity of phosphorene was studied via electrochemical measurements using a typical three-electrode configuration in the 0.1 M $HClO_4$ solution. Phosphorene was deposited on the glassy carbon electrode and dried under a vacuum to avoid degradation under an ambient atmosphere. Figure 5D shows the linear sweep voltammetry (LSV) curves of phosphorene and glassy carbon. As a comparison, the HER catalytic activity of phosphorene prepared from high-cost BP was also tested, as shown in Figure S10 (see the Supporting Information). The prepared phosphorene using low-cost BP showed a very negative onset potential compared with that prepared from high-cost BP. In the acidic solution, the HER always followed the Volmer−Heyrovsky reaction mechanism, which involves the discharge and H desorption processes. According to Zdeněk Sofer et al.'s work, the edge-plane BP showed a much higher catalytic activity than that of the basal BP.[50] In our work, we believe the higher catalytic activity on phosphorene low-cost BP is attributed to the higher amount of edge defects than that on phosphorene high-cost BP, which leads to more exposed active sites and also facilitates the charge transfer process. The phosphorene derived from low-cost BP shows a comparable HER catalytic activity and a low onset potential compared with those of previous literature results, indicating the promising potential of phosphorene for HER applications.[11,51] We are trying to increase their electrochemical activity and extend their applications by other methods such as element doping. Further detailed studies over these samples were out of the scope of our current paper, which will be performed in our following work. In addition to the application of BP as one HER catalyst, the prepared BP material can also be used as a promising anode material for lithium-ion and sodium-ion batteries due to its high theoretical capacity (2595 mAh/g) and low cost.[52] The application of the prepared BP in secondary batteries will be introduced in ourfuture work.

3. CONCLUSION

In summary, we have developed a modified CVT method with low-purity RP as a precursors to replace high-purity BP and realized the high-efficiency preparation of low-cost BP. To the best of our knowledge, this is the first work to show the successful preparation of high-quality BP from low-purity RP with a high conversion efficiency of around 97%. Additionally, the growth mechanism of low-cost and high-quality BP has been intensively studied, confirming that the impurities in low-purity RP cannot participate in the BP growth process. Furthermore, compared with the high-cost BP, the produced low-cost BP exhibits the same crystal quality and high-purity level, as well as local and electronic structures, making it suitable for application in nanophotonics, nanoelectronics, and energy storage. The exfoliated phosphorene nanosheets prepared from the low-cost BP show promising HER activity, producing the same performance as that of high-purity RP stating materials. Compared with the current high price of commercial BP crystals prepared from high-purity RP (around $600 (USD)/gram), this work can drastically reduce the cost of manufacturing by hundreds of times, showing promising potential in future scientific research and industrial applications.

■ ASSOCIATED CONTENT

Ⓢ Supporting Information

The Supporting Information is available free of charge at https://pubs.acs.org/doi/10.1021/acsanm.0c01101.

> Experimental Section, XRD patterns, Raman spectra, SEM images, EDX results, photographs of sealed silica ampoule, photographs of high-cost BP and low-cost BP, laboratory XPS survey spectra of low-cost BP, schematic illustration of the electrical conductivity measurement system, TEM images, and LSV curves of phosphorene catalyst (PDF)

■ AUTHOR INFORMATION

Corresponding Authors

Xueliang Sun − *Department of Mechanical and Materials Engineering, University of Western Ontario, London, Ontario N6A 5B9, Canada;* ⓘ orcid.org/0000-0003-0374-1245; Phone: +1-519-661-2111 Ext 87759; Email: xsun9@uwo.ca

Tsun-Kong Sham − *Department of Chemistry and Soochow-Western Centre for Synchrotron Radiation Research, University of Western Ontario, London, Ontario N6A 5B7, Canada;* ⓘ orcid.org/0000-0003-1928-6697; Phone: +1-519-661-2111 Ext 86341; Email: tsham@uwo.ca

Authors

Weihan Li − *Department of Mechanical and Materials Engineering and Department of Chemistry and Soochow-Western Centre for Synchrotron Radiation Research, University of Western Ontario, London, Ontario N6A 5B9, Canada*

Minsi Li − *Department of Mechanical and Materials Engineering and Department of Chemistry and Soochow-Western Centre for Synchrotron Radiation Research, University of Western Ontario, London, Ontario N6A 5B9, Canada*

Junjie Li − *Department of Mechanical and Materials Engineering, University of Western Ontario, London, Ontario N6A 5B9, Canada*

Jianneng Liang − *Department of Mechanical and Materials Engineering, University of Western Ontario, London, Ontario N6A 5B9, Canada*

Keegan R. Adair − *Department of Mechanical and Materials Engineering, University of Western Ontario, London, Ontario N6A 5B9, Canada*

Yongfeng Hu − *Canadian Light Source, Saskatoon, Saskatchewan S7N 2 V3, Canada*

Qunfeng Xiao − *Canadian Light Source, Saskatoon, Saskatchewan S7N 2 V3, Canada*

Xiaoyu Cui − *Canadian Light Source, Saskatoon, Saskatchewan S7N 2 V3, Canada*

Ruying Li − *Department of Mechanical and Materials Engineering, University of Western Ontario, London, Ontario N6A 5B9, Canada*

Frank Brandys − *3M Canada Company, London, Ontario N5 V 3R6, Canada*

Ranjith Divigalpitiya − *3M Canada Company, London, Ontario N5 V 3R6, Canada*

Complete contact information is available at:
https://pubs.acs.org/10.1021/acsanm.0c01101

Author Contributions

[#]W.L. and M.L. contributed equally to this work.

Notes

The authors declare no competing financial interest.

■ REFERENCES

(1) Bridgman, P. TWO NEW MODIFICATIONS OF PHOSPHORUS. *J. Am. Chem. Soc.* **1914**, *36* (7), 1344−1363.

(2) Ling, X.; Wang, H.; Huang, S.; Xia, F.; Dresselhaus, M. S. The renaissance of black phosphorus. *Proc. Natl. Acad. Sci. U. S. A.* **2015**, *112*, 201416581.

(3) Carvalho, A.; Wang, M.; Zhu, X.; Rodin, A. S.; Su, H.; Castro Neto, A. H. Phosphorene: from theory to applications. *Nature Reviews Materials* **2016**, *1* (11), 16061.

(4) Xia, F.; Wang, H.; Xiao, D.; Dubey, M.; Ramasubramaniam, A. Two-dimensional material nanophotonics. *Nat. Photonics* **2014**, *8* (12), 899.

(5) Li, L.; Yu, Y.; Ye, G. J.; Ge, Q.; Ou, X.; Wu, H.; Feng, D.; Chen, X. H.; Zhang, Y. Black phosphorus field-effect transistors. *Nat. Nanotechnol.* **2014**, *9* (5), 372.

(6) Eswaraiah, V.; Zeng, Q.; Long, Y.; Liu, Z. Black phosphorus nanosheets: synthesis, characterization and applications. *Small* **2016**, *12* (26), 3480−3502.

(7) Xia, F.; Wang, H.; Jia, Y. Rediscovering black phosphorus as an anisotropic layered material for optoelectronics and electronics. *Nat. Commun.* **2014**, *5*, 4458.

(8) Fei, R.; Faghaninia, A.; Soklaski, R.; Yan, J.-A.; Lo, C.; Yang, L. Enhanced thermoelectric efficiency via orthogonal electrical and thermal conductances in phosphorene. *Nano Lett.* **2014**, *14* (11), 6393−6399.

(9) Zhang, M.; Wu, Q.; Zhang, F.; Chen, L.; Jin, X.; Hu, Y.; Zheng, Z.; Zhang, H. 2D black phosphorus saturable absorbers for ultrafast photonics. *Adv. Opt. Mater.* **2019**, *7* (1), 1800224.

(10) Ren, X.; Zhou, J.; Qi, X.; Liu, Y.; Huang, Z.; Li, Z.; Ge, Y.; Dhanabalan, S. C.; Ponraj, J. S.; Wang, S.; et al. Few-Layer Black Phosphorus Nanosheets as Electrocatalysts for Highly Efficient Oxygen Evolution Reaction. *Adv. Energy Mater.* **2017**, *7* (19), 1700396.

(11) Shao, L.; Sun, H.; Miao, L.; Chen, X.; Han, M.; Sun, J.; Liu, S.; Li, L.; Cheng, F.; Chen, J. Facile preparation of NH 2-functionalized black phosphorene for the electrocatalytic hydrogen evolution reaction. *J. Mater. Chem. A* **2018**, *6* (6), 2494−2499.

(12) Wang, J.; Liu, D.; Huang, H.; Yang, N.; Yu, B.; Wen, M.; Wang, X.; Chu, P. K.; Yu, X. F. In-Plane Black Phosphorus/Dicobalt Phosphide Heterostructure for Efficient Electrocatalysis. *Angew. Chem.* **2018**, *130* (10), 2630−2634.

(13) Zhou, Y.; Zhang, M.; Guo, Z.; Miao, L.; Han, S.-T.; Wang, Z.; Zhang, X.; Zhang, H.; Peng, Z. Recent advances in black phosphorus-based photonics, electronics, sensors and energy devices. *Mater. Horiz.* **2017**, *4* (6), 997−1019.

(14) Tian, Y.; Wang, H.; Li, H.; Guo, Z.; Tian, B.; Cui, Y.; Li, Z.; Li, G.; Zhang, H.; Wu, Y. Recent advances in black phosphorus/carbon hybrid composites: from improved stability to applications. *J. Mater. Chem. A* **2020**, *8* (9), 4647−4676.

(15) Tian, B.; Tian, B.; Smith, B.; Scott, M.; Lei, Q.; Hua, R.; Tian, Y.; Liu, Y. Facile bottom-up synthesis of partially oxidized black phosphorus nanosheets as metal-free photocatalyst for hydrogen evolution. *Proc. Natl. Acad. Sci. U. S. A.* **2018**, *115* (17), 4345−4350.

(16) Zhu, X.; Zhang, T.; Sun, Z.; Chen, H.; Guan, J.; Chen, X.; Ji, H.; Du, P.; Yang, S. Black phosphorus revisited: a missing metal-free elemental photocatalyst for visible light hydrogen evolution. *Adv. Mater.* **2017**, *29* (17), 1605776.

(17) Favron, A.; Gaufrès, E.; Fossard, F.; Phaneuf-L'Heureux, A.-L.; Tang, N. Y.; Lévesque, P. L.; Loiseau, A.; Leonelli, R.; Francoeur, S.; Martel, R. Photooxidation and quantum confinement effects in exfoliated black phosphorus. *Nat. Mater.* **2015**, *14* (8), 826.

(18) Gusmao, R.; Sofer, Z.; Pumera, M. Black phosphorus rediscovered: From bulk material to monolayers. *Angew. Chem., Int. Ed.* **2017**, *56* (28), 8052−8072.

(19) Zhou, Q.; Chen, Q.; Tong, Y.; Wang, J. Light-Induced ambient degradation of few-layer black phosphorus: mechanism and protection. *Angew. Chem., Int. Ed.* **2016**, *55* (38), 11437−11441.

(20) Abellan, G.; Wild, S.; Lloret, V.; Scheuschner, N.; Gillen, R.; Mundloch, U.; Maultzsch, J.; Varela, M.; Hauke, F.; Hirsch, A. Fundamental Insights into the Degradation and Stabilization of Thin Layer Black Phosphorus. *J. Am. Chem. Soc.* **2017**, *139* (30), 10432−10440.

(21) Zhang, T.; Wan, Y.; Xie, H.; Mu, Y.; Du, P.; Wang, D.; Wu, X.; Ji, H.; Wan, L. Degradation Chemistry and Stabilization of Exfoliated Few-Layer Black Phosphorus in Water. *J. Am. Chem. Soc.* **2018**, *140*, 7561.

(22) Ryder, C. R.; Wood, J. D.; Wells, S. A.; Yang, Y.; Jariwala, D.; Marks, T. J.; Schatz, G. C.; Hersam, M. C. Covalent functionalization and passivation of exfoliated black phosphorus via aryl diazonium chemistry. *Nat. Chem.* **2016**, *8* (6), 597.

(23) Yang, B.; Wan, B.; Zhou, Q.; Wang, Y.; Hu, W.; Lv, W.; Chen, Q.; Zeng, Z.; Wen, F.; Xiang, J.; et al. Te-Doped Black Phosphorus Field-Effect Transistors. *Adv. Mater.* **2016**, *28* (42), 9408−9415.

(24) Shirotani, I.; Maniwa, R.; Sato, H.; Fukizawa, A.; Sato, N.; Maruyama, Y.; Kajiwara, T.; Inokuchi, H.; Akimoto, S. PREPARATION, GROWTH OF LARGE SINGLE-CRYSTALS, AND PHYSICOCHEMICAL PROPERTIES OF BLACK PHOSPHORUS AT HIGH-PRESSURES AND TEMPERATURES. *Nippon Kagaku Kaishi* **1981**, No. 10, 1604−1609.

(25) Endo, S.; Akahama, Y.; Terada, S.-i.; Narita, S.-i. Growth of large single crystals of black phosphorus under high pressure. *Jpn. J. Appl. Phys.* **1982**, *21* (8A), L482.

(26) Krebs, H.; Weitz, H.; Worms, K. Über die struktur und eigenschaften der halbmetalle. Viii. Die katalytische darstellung des schwarzen phosphors. *Z. Anorg. Allg. Chem.* **1955**, *280* (1−3), 119−133.

(27) Brown, A.; Rundqvist, S. Refinement of the crystal structure of black phosphorus. *Acta Crystallogr.* **1965**, *19* (4), 684−685.

(28) Lange, S.; Schmidt, P.; Nilges, T. Au3SnP7@ black phosphorus: an easy access to black phosphorus. *Inorg. Chem.* **2007**, *46* (10), 4028−4035.

(29) Nilges, T.; Kersting, M.; Pfeifer, T. A fast low-pressure transport route to large black phosphorus single crystals. *J. Solid State Chem.* **2008**, *181* (8), 1707−1711.

(30) Köpf, M.; Eckstein, N.; Pfister, D.; Grotz, C.; Krüger, I.; Greiwe, M.; Hansen, T.; Kohlmann, H.; Nilges, T. Access and in situ growth of phosphorene-precursor black phosphorus. *J. Cryst. Growth* **2014**, *405*, 6−10.

(31) Xu, Y.; Shi, X.; Zhang, Y.; Zhang, H.; Zhang, Q.; Huang, Z.; Xu, X.; Guo, J.; Zhang, H.; Sun, L.; et al. Epitaxial nucleation and lateral growth of high-crystalline black phosphorus films on silicon. *Nat. Commun.* **2020**, *11* (1), 1−8.

(32) Zhao, M.; Qian, H.; Niu, X.; Wang, W.; Guan, L.; Sha, J.; Wang, Y. Growth mechanism and enhanced yield of black phosphorus microribbons. *Cryst. Growth Des.* **2016**, *16* (2), 1096−1103.

(33) Zhang, Z.; Xin, X.; Yan, Q.; Li, Q.; Yang, Y.; Ren, T.-L. Two-step heating synthesis of sub-3 millimeter-sized orthorhombic black phosphorus single crystal by chemical vapor transport reaction method. *Science china materials* **2016**, *59* (2), 122−134.

(34) Zhao, M.; Niu, X.; Guan, L.; Qian, H.; Wang, W.; Sha, J.; Wang, Y. Understanding the growth of black phosphorus crystals. *CrystEngComm* **2016**, *18* (40), 7737−7744.

(35) Shriber, P.; Samanta, A.; Nessim, G. D.; Grinberg, I. First-Principles Investigation of Black Phosphorus Synthesis. *J. Phys. Chem. Lett.* **2018**, *9* (7), 1759−1764.

(36) Mayorga-Martinez, C. C.; Sofer, Z.; Sedmidubský, D.; Luxa, J.; Kherzi, B.; Pumera, M. Metallic impurities in black phosphorus nanoflakes prepared by different synthetic routes. *Nanoscale* **2018**, *10* (3), 1540−1546.

(37) Li, W.-J.; Chou, S.-L.; Wang, J.-Z.; Liu, H.-K.; Dou, S.-X. Simply mixed commercial red phosphorus and carbon nanotube composite with exceptionally reversible sodium-ion storage. *Nano Lett.* **2013**, *13* (11), 5480−5484.

(38) Ansari, S. A.; Ansari, M. S.; Cho, M. H. Metal free earth abundant elemental red phosphorus: a new class of visible light photocatalyst and photoelectrode materials. *Phys. Chem. Chem. Phys.* **2016**, *18* (5), 3921−3928.

(39) Corbridge, D. E. *Phosphorus: Chemistry, Biochemistry and Technology*; CRC Press, 2016.

(40) Keyes, R. W. The electrical properties of black phosphorus. *Phys. Rev.* **1953**, *92* (3), 580.

(41) Warschauer, D. Electrical and optical properties of crystalline black phosphorus. *J. Appl. Phys.* **1963**, *34* (7), 1853−1860.

(42) Xu, Y.; Yuan, J.; Fei, L.; Wang, X.; Bao, Q.; Wang, Y.; Zhang, K.; Zhang, Y. Selenium-doped black phosphorus for high-responsivity 2D photodetectors. *Small* **2016**, *12* (36), 5000−5007.

(43) Lv, W.; Yang, B.; Wang, B.; Wan, W.; Ge, Y.; Yang, R.; Hao, C.; Xiang, J.; Zhang, B.; Zeng, Z.; Liu, Z. Sulfur-doped black phosphorus field-effect transistors with enhanced stability. *ACS Appl. Mater. Interfaces* **2018**, *10* (11), 9663−9668.

(44) Lin, F.; Liu, Y.; Yu, X.; Cheng, L.; Singer, A.; Shpyrko, O. G.; Xin, H. L.; Tamura, N.; Tian, C.; Weng, T.-C.; et al. Synchrotron X-ray analytical techniques for studying materials electrochemistry in rechargeable batteries. *Chem. Rev.* **2017**, *117* (21), 13123−13186.

(45) Li, W.; Li, M.; Hu, Y.; Lu, J.; Lushington, A.; Li, R.; Wu, T.; Sham, T. K.; Sun, X. Synchrotron-Based X-ray Absorption Fine Structures, X-ray Diffraction, and X-ray Microscopy Techniques Applied in the Study of Lithium Secondary Batteries. *Small Methods* **2018**, *2*, 1700341.

(46) Edmonds, M.; Tadich, A.; Carvalho, A.; Ziletti, A.; O'Donnell, K.; Koenig, S.; Coker, D.; Ozyilmaz, B.; Neto, A. C.; Fuhrer, M. Creating a stable oxide at the surface of black phosphorus. *ACS Appl. Mater. Interfaces* **2015**, *7* (27), 14557−14562.

(47) Nicotra, G.; Politano, A.; Mio, A.; Deretzis, I.; Hu, J.; Mao, Z.; Wei, J.; La Magna, A.; Spinella, C. Absorption edges of black phosphorus: A comparative analysis. *Phys. Status Solidi B* **2016**, *253* (12), 2509−2514.

(48) Farrell, S. P.; Fleet, M. E.; Stekhin, I. E.; Kravtsova, A.; Soldatov, A. V.; Liu, X. Evolution of local electronic structure in alabandite and niningerite solid solutions [(Mn, Fe) S,(Mg, Mn) S, (Mg, Fe) S] using sulfur K-and L-edge XANES spectroscopy. *Am. Mineral.* **2002**, *87* (10), 1321−1332.

(49) Li, W.; Wang, Z.; Zhao, F.; Li, M.; Gao, X.; Zhao, Y.; Wang, J.; Zhou, J.; Hu, Y.; Xiao, Q.; et al. Phosphorene Degradation: Visualization and Quantification of Nanoscale Phase Evolution by Scanning Transmission X-ray Microscopy. *Chem. Mater.* **2020**, *32* (3), 1272−1280.

(50) Sofer, Z.; Sedmidubský, D.; Huber, Š.; Luxa, J.; Bouša, D.; Boothroyd, C.; Pumera, M. Layered Black Phosphorus: Strongly Anisotropic Magnetic, Electronic, and Electron-Transfer Properties. *Angew. Chem., Int. Ed.* **2016**, *55* (10), 3382−3386.

(51) He, R.; Hua, J.; Zhang, A.; Wang, C.; Peng, J.; Chen, W.; Zeng, J. Molybdenum Disulfide−Black Phosphorus Hybrid Nanosheets as a Superior Catalyst for Electrochemical Hydrogen Evolution. *Nano Lett.* **2017**, *17* (7), 4311−4316.

(52) Qiu, M.; Sun, Z.; Sang, D.; Han, X.; Zhang, H.; Niu, C. Current progress in black phosphorus materials and their applications in electrochemical energy storage. *Nanoscale* **2017**, *9* (36), 13384−13403.